

the Renner-Teller perturbed 1B_1 levels which, as discussed above, are presumed to form the background of weak transitions responsible for the continuum. Mechanism ii directly couples the 1A_2 and 3B_2 states and will therefore involve all 1A_2 levels, including those that have relatively pure 1B_1 character (entry 2 in Table VII). Thus, if mechanism ii is operative, the levels sampled in the present work derive their ~ 10 - 50 - μ s lifetimes, at least in part, from spin-orbit coupling to the triplet manifold.

Acknowledgment. This research has been supported by the National Science Foundation Grants CHE-79-25451 and CHE-82-17121 at the University of California at Irvine. Partial support for the collisional relaxation study by the Department of Energy (Office of Basic Energy Sciences) Contract DE-AT-03-76-ER-70217 is gratefully acknowledged.

Registry No. SO_2 , 7446-09-5.

Kinetics and Mechanism of the $CH + N_2$ Reaction. Temperature- and Pressure-Dependence Studies and Transition-State-Theory Analysis

Michael R. Berman*[†] and M. C. Lin*

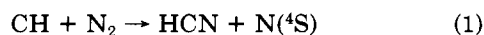
Chemistry Division, Naval Research Laboratory, Washington, D.C. 20375 (Received: January 10, 1983)

The reaction $CH + N_2 \rightarrow$ products was studied at 297 K at total pressures between 25 and 787 torr. The second-order reaction rate constant was found to be pressure dependent, varying by a factor of 9.6 in this range. This reaction was also studied in the range 297-675 K at 100-torr total pressure. The rate constant decreases with increasing temperature and cannot be adequately described by a linear fit in this range. Transition-state-RRKM-theory calculations for the reaction proceeding through a long-lived intermediate, HCN_2 , successfully describe the data. Stabilization of the adduct is the primary reaction channel at lower temperatures while metathesis dominates above 1000 K. These calculations provide a consistent description of these and previous data from flame studies.

I. Introduction

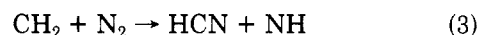
The reaction of CH with N_2 is of considerable importance due to its role in the chemistry of planetary atmospheres and hydrocarbon flames. This reaction is included in models of both the chemistry of the nitrogen- and hydrocarbon-rich atmosphere of Titan¹ and the production of nitric oxide in hydrocarbon flame fronts.²⁻⁵ The $CH + N_2$ reaction is alluring to modelers of such systems in that it represents the least endoergic pathway for a hydrocarbon fragment to break the $N\equiv N$ bond enabling the incorporation of N atoms and other nitrogen-containing compounds into subsequent reaction schemes. A clear understanding of the kinetics and mechanisms of this basic reaction is critical for evaluating the complex systems typically found in atmospheric and combustion environments.

Recent interest in the $CH + N_2$ reaction has been part of an effort to unravel the mechanism of NO formation in hydrocarbon/air flames. The production of NO in these hydrocarbon flame fronts cannot be described by the Zeldovich mechanism⁶ which successfully accounts for NO production in the postcombustion region. Fenimore² proposed the reactions of carbon or hydrocarbon radicals with N_2



followed by oxidation of the products to account for the production of NO in the reaction zone of these flames. Blauwens et al.,³ using molecular beam sampling with

mass-spectrometric detection to measure absolute radical and molecule concentrations, found that the production of this so-called "prompt" NO could be represented by either reaction 1 or 3. They evaluated rate constants for



each process finding activation energies of 11.0 and 22.5 kcal/mol, respectively, noting that these values are applicable only if the observed NO was produced solely by the reaction considered. Matsui and Nomaguchi⁴ found that the amount of prompt NO is proportional to the CH radical concentration and evaluated a rate constant for reaction 1 having an activation energy of 13.6 kcal/mol. However, they detected CH radicals indirectly and did not consider CH_2 radicals. Miyauchi et al.⁷ found that HCN was formed prior to the prompt NO, supporting reactions 1 and/or 3. In this case, they did not include reaction 1 in their analysis due to the spin change involved. They used instead reaction 3 as the source of HCN and evaluated a rate constant for this reaction having an activation energy of 35.2 kcal/mol. The objection to reaction 1 on the grounds of spin consideration, however, has been

(1) D. F. Strobel, *Planet. Space Sci.*, **30**, 839 (1982).

(2) C. P. Fenimore, "13th Symposium (International) on Combustion", The Combustion Institute, Pittsburgh, PA, 1971, p 373.

(3) J. Blauwens, B. Smets, and J. Peeters, "16th Symposium (International) on Combustion", The Combustion Institute, Pittsburgh, PA, 1977, p 1055.

(4) Y. Matsui and T. Nomaguchi, *Combust. Flame*, **32**, 205 (1978).

(5) J. Duterque, N. Avezard, and R. Borghi, *Combust. Sci. Technol.*, **25**, 85 (1981).

(6) Ya. B. Zeldovich, *Acta Physicochim. URSS*, **21**, 577 (1946).

(7) T. Miyauchi, Y. Mori, and A. Imamura, "16th Symposium (International) on Combustion", The Combustion Institute, Pittsburgh, PA, 1977, p 1073.

*NRC/NRL Postdoctoral Research Associate (1981-1982). Present address: McDonnell Douglas Research Laboratories, St. Louis, MO 63166.

previously refuted.^{8,9} Benson⁹ has also argued against the importance of reaction 3 on structural and thermochemical grounds. On the basis of calculations, Duterque et al.⁵ concluded that both reactions 1 and 3 can contribute to prompt NO formation under different flame conditions.

In addition to the work in flames, room-temperature studies of the above reactions have been carried out. The reaction of CH₂(X³B₁) with N₂ was studied by Laufer and Bass,¹⁰ who found a rate constant of $\leq 10^{-16}$ cm³ molecule⁻¹ s⁻¹. HCN was produced on a millisecond time scale through an undetermined mechanism. The reaction of CH + N₂ has been studied by several groups. Braun et al.¹¹ and Bosnali and Perner,¹² each monitoring CH(X²Π) by its absorption at 314 nm, found rate constants differing by a factor of 14. Butler et al.,⁸ using 193-nm laser photolysis to generate CH radicals and laser-induced fluorescence (LIF) detection, determined a rate constant similar to that of Bosnali and Perner and noted that the rate constant is pressure dependent, indicating that the reaction proceeds through a long-lived intermediate. More recently, Wagal et al.,¹³ producing CH by infrared multiphoton dissociation and using LIF detection, confirmed the pressure dependence and found a somewhat smaller rate constant than that determined by Butler et al.⁸ at a similar pressure.

It is clear that a better understanding of the reactions of small hydrocarbon radicals with N₂ is needed. Despite studies at room temperature and in flames, a consistent picture of the fundamental reaction of CH with N₂ has not yet emerged. The experimentally determined room-temperature rate constants are many orders of magnitude larger than those extrapolated to room temperature from work in flames between 1500 and 2000 K if the activation energy of 11 kcal/mol determined by Blauwens et al.³ is applicable. In an effort to resolve some of these uncertainties and apparent inconsistencies, we have undertaken a detailed study of this reaction using laser photolysis of CHBr₃ at 266 nm to generate CH radicals which were detected by their LIF. The rate constant for this reaction was measured in the range 297–675 K and the pressure dependence was studied at 297 K between total pressures of 25 and 787 torr. The results are analyzed by using the transition-state (RRKM) theory.

II. Experimental Section

The experimental apparatus and technique used are well established and have been described in detail elsewhere.¹⁴ Briefly, the output of a Nd:YAG laser was frequency quadrupled and the 266-nm radiation (2–5 mJ) was focused with a 50 cm focal length BaF₂ lens through baffled arms into the center of the Pyrex reaction cell. The output of a Nd:YAG laser pumped dye laser (Coumarin 120, ~8 ns, 50–100 μJ, 10 Hz) passed collinear with and counter-propagating to the photolysis beam at a variable time delay (–5 to +300 μs) relative to the photolysis pulse. LIF excited by the dye laser from the A²Δ → X²Π, R_{1(cd,dc)} (2) transition of the (0,0) band in CH at 429.8 nm was collected

by *f*/3 optics, filtered to pass CH fluorescence, and detected by an RCA 1P28 photomultiplier tube. Five laser shots, each corrected for scattered light and background, were averaged at each time delay and stored on a computer (HP 9825A). The time delay was stepped in 1-μs intervals and the signal followed typically through 2–3 lifetimes.

The reaction cell was resistively heated and the temperature measured in the reaction zone before and after the experiments and 1 cm off the laser beam axis during the experiments by a retractable Fe–constantan thermocouple. Temperatures were constant to ±0.5 K over the course of a rate constant determination. The CH precursors, CHBr₃, diluted in Ar, N₂, and Ar buffer gas, were mixed and slowly flowed through the cell. The CHBr₃ pressure was typically ≤1 mtorr. Temperature-dependent studies were carried out at a total pressure of 100 torr. In all studies, the total pressure was maintained by the addition of Ar buffer gas which thermalized the reactants and limited diffusion out of the viewing zone. Concentrations of reactants were determined by their partial pressures in the flowing mixture. All pressures were measured by capacitance manometers (MKS Baratron 0–100- and 0–1000-torr heads).

CHBr₃ (Aldrich) was distilled from 273 to 195 K and degassed before use. Nitrogen (Matheson, prepurified, 99.998% minimum) and Ar (99.995%) were used without further purification.

III. Data Analysis

The LIF intensity from CH was taken as a relative measure of the CH(X²Π) concentration. After initial relaxation effects, the LIF signal decayed exponentially as a function of delay time, *t*, after the photolysis pulse and was least-squares fitted to the equation

$$I = Ae^{-k_1 t} + B \quad (4)$$

where *k*₁ is the pseudo-first-order-decay rate constant for CH LIF due to all loss processes, i.e., reaction and diffusion out of the beam. The LIF signal was fitted over at least two lifetimes.

The decay rate constant increased proportionally to the concentration of added N₂. Second-order rate constants, *k*₂, for the CH + N₂ → products reaction at a given temperature and total pressure were obtained by weighted, linear least-squares fits to the equation

$$k_1 = k_n + k_2[N_2] \quad (5)$$

where *k*_n is the loss rate constant for CH due to reaction and diffusion in the absence of N₂.

Since the rate constant for the reaction of CH + N₂ is pressure dependent, the observed *k*₁'s can also be analyzed in terms of a third-order rate constant according to

$$k_1 = k_n + k_3^{sc} P \{ \beta_{c,Ar} X_{Ar} + \beta_{c,N_2} X_{N_2} \} [N_2] \quad (6)$$

where *X*_{*i*} and β_{*c,i*} are the mole fraction and the collisional efficiency (i.e., the fraction of collisions that lead to stabilization) of substituent *i*, and *P* is the total pressure. *k*_{3^{sc}} is the third-order rate constant in the strong-collision limit in which each collision leads to stabilization of the adduct. The third-order rate constant, *k*₃, is defined as

$$k_3 = k_3^{sc} \beta_c \quad (7)$$

The relative collision efficiencies of Ar and N₂ can be analyzed by rearranging eq 6 to give

$$(k_1 - k_n) / [N_2] = k_3^{sc} P \{ \beta_{c,Ar} + (\beta_{c,N_2} - \beta_{c,Ar}) X_{N_2} \} \quad (8)$$

where the mole fraction of CHBr₃ is neglected due to its

(8) J. E. Butler, J. W. Fleming, L. P. Goss, and M. C. Lin, *Chem. Phys.*, **56**, 355 (1981).

(9) S. W. Benson, "16th Symposium (International) on Combustion", The Combustion Institute, Pittsburgh, PA, 1977, p 1062.

(10) A. H. Laufer and A. M. Bass, *Combust. Flame*, **32**, 215 (1978).

(11) W. Braun, J. R. McNesby, and A. M. Bass, *J. Chem. Phys.*, **46**, 2071 (1971).

(12) M. W. Bosnali and D. Perner, *Z. Naturforsch. A*, **26**, 1768 (1971).

(13) S. S. Wagal, T. Carrington, S. V. Filseth, and C. M. Sadowski, *Chem. Phys.*, **69**, 61 (1982).

(14) M. R. Berman, J. W. Fleming, A. B. Harvey, and M. C. Lin, "19th Symposium (International) on Combustion", The Combustion Institute, Pittsburgh, PA, 1982, p 73.

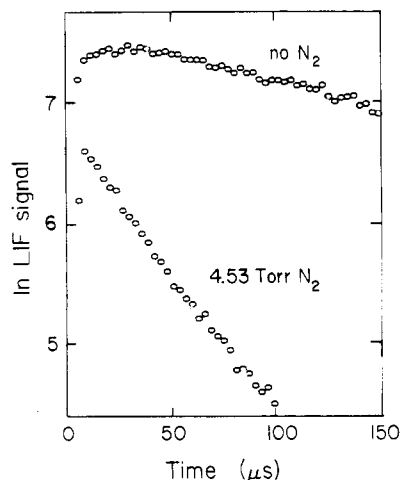


Figure 1. Typical laser-induced fluorescence profiles of CH radicals ($A^2\Delta-X^2II$) vs. time between the photolysis laser (266 nm) and the probe laser (429.8 nm). The temperature was 319 K and the photolysis energy was 3 mJ/pulse. For clarity, the traces are offset and only every third data point is shown. The pressures were ~ 100 torr of Ar, 0.2 mtorr of $CHBr_3$ and in the upper curve, no reactant gas, and in the lower curve, 4.53 torr of N_2 .

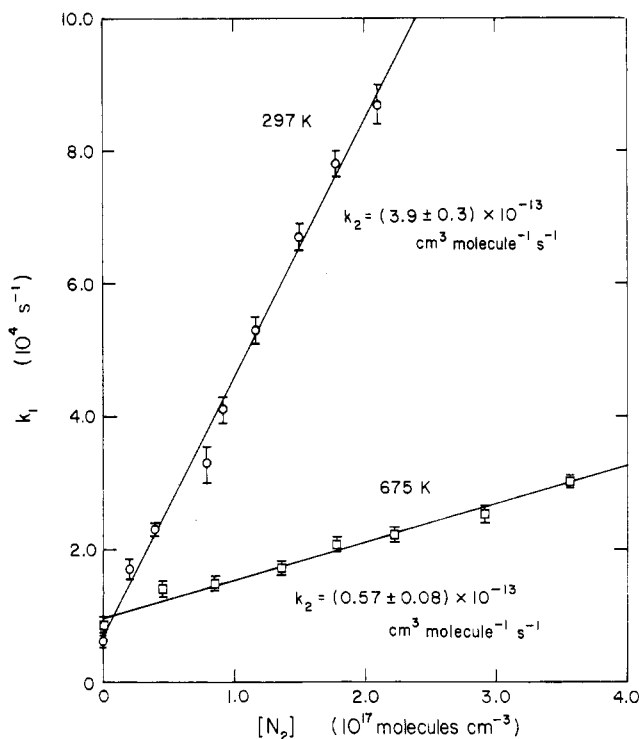


Figure 2. Plot of first-order decay constants for CH radicals vs. the concentration of N_2 at 297 and 675 K. The slopes of these plots are the listed second-order bimolecular rate constants for the reaction of $CH + N_2$ at the appropriate temperature and 100-torr total pressure. The intercept is the rate constant for loss of CH due to other reactions and diffusion out of the viewing region. Error bars shown are the standard deviation in the exponential fits for k_1 .

very low concentration. In the case where the collisional efficiencies are equal ($\beta_{c,Ar} = \beta_{c,N_2} = \beta_c$), the third-order rate constant can be obtained from

$$(k_1 - k_n)/[N_2]^2 = k_3^{\text{sc}}\beta_c([Ar]/[N_2] + 1) \quad (9)$$

where now $k_3^{\text{sc}}\beta_c = k_2/[M]$ and $[M]$ is the concentration of all collision partners.

The temperature dependence of the measured second-order rate constants was analyzed by a simple Arrhenius expression.

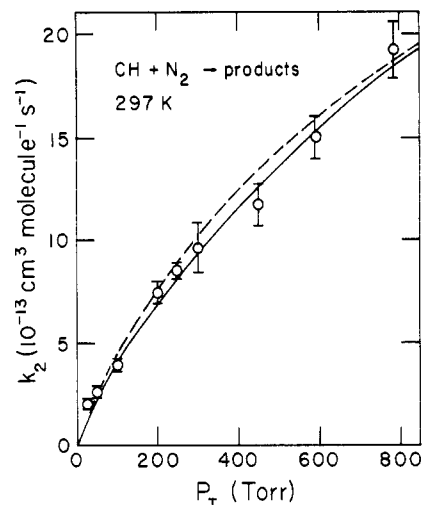


Figure 3. Plot of the second-order rate constant for the $CH + N_2$ reaction vs. total pressure at 297 K. The curves are the results of transition-state-theory calculations of k using parameter set I for the solid curve and parameter set III for the dashed curve.

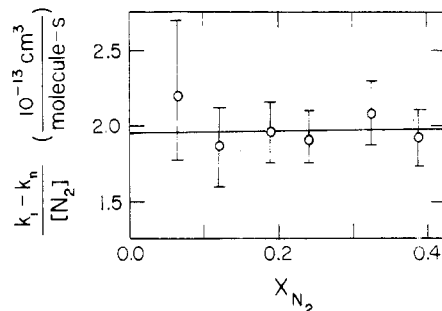


Figure 4. Plot of $(k_1 - k_n)/[N_2]$ vs. the mole fraction of N_2 for the experiments at 297 K with a total pressure of 25 torr. The slope is zero within experimental error.

TABLE I: Rate Constants for the Reaction

$CH + N_2 \xrightarrow{k_2} \text{Products}$ as a Function of Total Pressure at 297 K

P , torr	no. of concn	$10^{13}k_2$, $\text{cm}^3 \text{ molecule}^{-1} \text{ s}^{-1}$	$10^{31}k_2/[M]$, $\text{cm}^6 \text{ molecule}^{-2} \text{ s}^{-1}$
25	7	2.0 ± 0.15	2.5 ± 0.2
50	9	2.6 ± 0.2	1.6 ± 0.1
100	9	3.9 ± 0.3	1.2 ± 0.1
200	8	7.4 ± 0.5	1.14 ± 0.08
250	6	8.5 ± 0.4	1.05 ± 0.05
300	9	9.6 ± 1.2	0.99 ± 0.12
450	6	11.7 ± 1.0	0.80 ± 0.07
595	8	15.0 ± 1.0	0.78 ± 0.05
787	6	19.2 ± 0.7	0.75 ± 0.03

IV. Results

Typical plots of the natural logarithm of the CH LIF signal vs. delay time are shown in Figure 1. The slopes of these plots give the first-order rate constants, k_1 . Second-order rate constants, k_2 , for a given temperature and pressure are obtained by plotting k_1 vs. N_2 concentration as shown in Figure 2. Second-order rate constants were determined at 297 K for total pressures between 25 and 787 torr. These values are displayed in Figure 3 and are summarized in Table I. The errors listed for k_2 are 1σ .

The data from which the second-order rate constants were obtained were also analyzed according to eq 8 in order to determine the relative collision efficiencies of Ar and N_2 . Relative efficiencies are most accurately determined

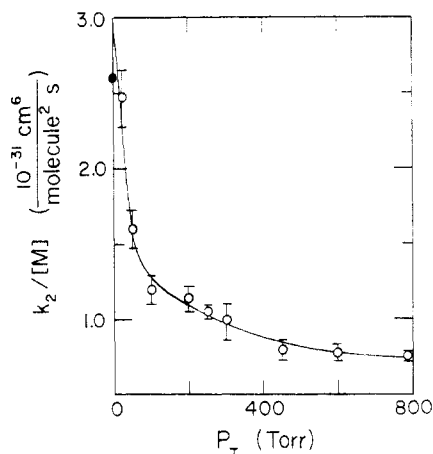


Figure 5. Plot of the third-order rate constant for the CH + N₂ reaction vs. total pressure at 297 K. The open circles are the data from this work. The filled circle is the low-pressure limiting rate constant determined by Wagal et al.¹³

TABLE II: Rate Constant for the Reaction

CH + N₂ $\xrightarrow{k_2}$ Products as a Function of Temperature at 100-torr Total Pressure

T, K	no. of concn	10 ¹³ k ₂ , cm ³ molecule ⁻¹ s ⁻¹
297	9	3.9 ± 0.3
319	6	3.7 ± 0.2
379	6	2.4 ± 0.1
471	6	1.3 ± 0.15
675	8	0.57 ± 0.08

when there is a wide variation in the N₂ mole fraction, i.e., experiments at low total pressure. Figure 4 shows the data at 25-torr total pressure plotted according to eq 8. The slope is zero within experimental error, indicating that the collisional efficiencies of Ar and N₂ are effectively equal in these experiments, i.e., β_{c,Ar} = β_{c,N₂} = β_c.

Since the collisional efficiencies are equal, third-order rate constants can be evaluated according to eq 9. In all cases, these rate constants were equal to k₂/[M] within experimental errors. The former had considerably larger error limits due to subtraction of k_n from each k₁. As a result, the latter values were used. They are listed in Table I and plotted vs. total pressure in Figure 5. This curve can be extrapolated to give a low-pressure limiting rate constant of k₀ = (2.8 ± 0.5) × 10⁻³¹ cm⁶ molecule⁻² s⁻¹. This figure also shows the low-pressure limiting rate constant determined by Wagal et al.,¹³ k₀ = 2.6 × 10⁻³¹ cm⁶ molecule⁻² s⁻¹.

The second-order rate constants were determined in the temperature range 297–675 K at a total pressure of 100 torr. These rate constants are listed in Table II and are plotted in Arrhenius form in Figure 6. A weighted, linear least-squares fit to these rate constants gave k = [(1.7 ± 0.3) × 10⁻¹⁴] exp[(1950 ± 130)/RT] cm³ molecule⁻¹ s⁻¹ with the activation energy in units of cal/mol. The linear fit, however, fails to adequately describe the data at the lowest and highest temperatures studied.

V. Theoretical Calculation of Rate Constants

Transition-State Theory—RRKM Model. The observed temperature and pressure dependence for the reaction of CH + N₂ suggests that the reaction takes place, at least in part, through an intermediate complex. As shown in the mechanism below, the HCN₂ adduct initially formed with a great deal of vibrational excitation can decompose to either reactants (channel 10b) or, if initial excitation is sufficient, to new products (channel 10c) or it can be

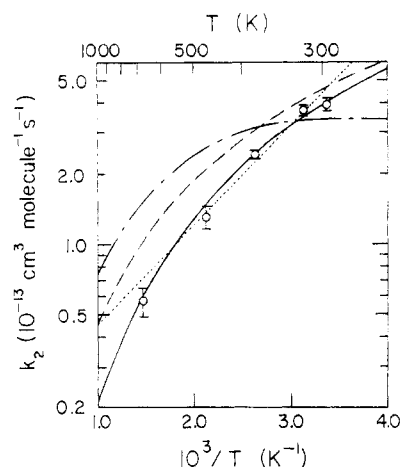
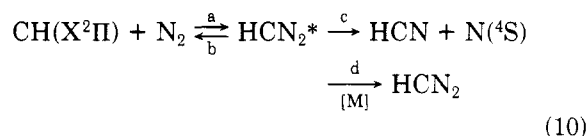


Figure 6. Second-order rate constant for the CH + N₂ reaction at 100-torr total pressure plotted in Arrhenius form. The dotted line (···) is a linear least-squares fit to the data. The curves are the results of transition-state-theory calculations using the following: curve a (—), parameter set II; curve b (---), parameter set V; curve c (---), parameter set IV.

stabilized by collisions (channel 10d).



The experimentally observed rate constant for the disappearance of CH, k_{loss}, is given in the steady-state approximation for [HCN₂*] by

$$k_{\text{loss}} = \frac{-d[\text{CH}]/dt}{[\text{CH}][\text{N}_2]} = \frac{k_b K_{ab}(k_c + k_d[\text{M}])}{k_b + k_c + k_d[\text{M}]} \quad (11)$$

where K_{ab} = k_a/k_b is the equilibrium constant between reactions 10a and 10b.

Using transition-state theory with the application of RRKM theory to the unimolecular decomposition of the chemically activated HCN₂* intermediate, one can express k_{loss} for the general case of reactants A and B at reaction temperature T (see Appendix) as

$$k_{\text{loss}} = \frac{\alpha \kappa_b}{h} \frac{q_{\text{tr}}^\ddagger}{q_A q_B} e^{-E_a/RT} \int_0^\infty \frac{(\omega + k_E') \sum P(E^+)}{k_E + k_E' + \omega} e^{-E^+/RT} dE^+ \quad (12)$$

where k_E and k_{E'} are the energy-specific reaction probabilities for channels 10b and 10c and the rate constant for stabilization of the adduct is ω. The energy-specific rate constants for unimolecular decomposition of the adduct are given by RRKM theory¹⁵ using a simple treatment of adiabatic rotations as

$$k_E = l_b I_b \kappa_b \frac{\sum P(E^+)}{hN(E)} \quad (13a)$$

$$k_{E'} = l_c I_c \kappa_c \frac{\sum P(E^+ + \Delta E_a + \Delta E_0)}{hN(E)} \quad (13b)$$

where ∑P(E⁺) is the sum of vibrational states of the transition state b at energy E⁺ and N(E) is the density of vibrational states of the adduct at energy E with these

(15) P. J. Robinson and K. A. Holbrook, "Unimolecular Reactions", Wiley, New York, 1972.

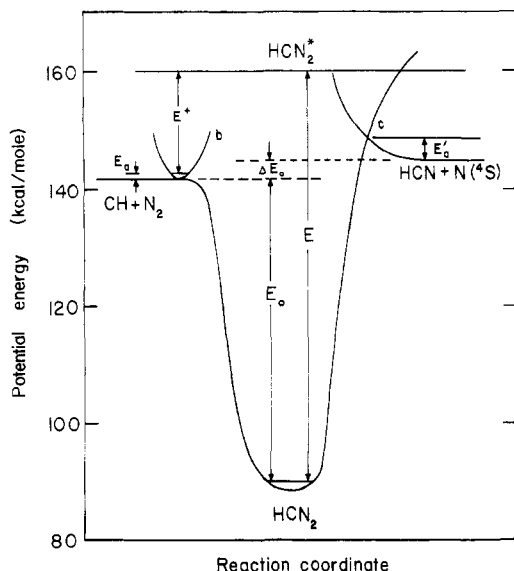


Figure 7. Potential energy diagram for the CH + N₂ system. The activation energy to production of HCN + N(*S) is determined by the crossing of the doublet and quartet surfaces of the adduct. Transition states are denoted by b and c. $\Delta E_a = E_a' - E_a$.

energies defined in Figure 7. Primed quantities refer to reaction channel or transition state c. The superscripts * and † refer to the stable adduct and a transition state, respectively. The ratio of overall rotational partition functions without symmetry numbers for the transition state b and the adduct is given by $I_b = q^\dagger/q^*$, while the statistical factor¹⁶ and transmission coefficient for reaction path 10b are given by l_b and κ_b , respectively. I_c , l_c , and κ_c are similar quantities for reaction path 10c. The total partition functions for reactants A and B excluding symmetry numbers and electronic degrees of freedom are given by q_A and q_B while q_{tr}^\dagger is the product of translational and rotational partition functions for the transition state of channel 10b. Electronic multiplicities for reactants A and B and the adduct, g_A , g_B , and g_{AB}^* , respectively, and the statistical factor for reaction path 10a are contained in $\alpha = l_a g_{AB}^*/g_A g_B$. Additional reaction channels can easily be incorporated into eq 12 as needed.

The rate constant for stabilization of the excited adduct is given in the weak-collision approximation by $\omega = k_d[M]$ where $k_d = \beta_c Z_{LJ}$ and Z_{LJ} is the Lennard-Jones collision frequency of the adduct at unit concentration of bath gas M and β_c (the subscript does not refer to channel 10c) is the collision efficiency defined by Troe¹⁷ for thermally activated systems. The efficiency of collisions between the adduct and some collision partner can be determined from $\langle \Delta E \rangle$, the average energy transferred in all transitions (up and down) according to the relationship¹⁷

$$\frac{\beta_c}{1 - \beta_c^{1/2}} \cong \frac{-\langle \Delta E \rangle}{F_E kT} \quad (14)$$

The calculation of absolute rate constants on the basis of eq 12 requires knowledge of molecular properties of the adduct and the transition states such as moments of inertia, hence geometries, sets of vibrational frequencies, and E_0 , the energy barrier to dissociation of the adduct relative to the reactants. Due to the difficulty of experimentally determining these quantities, empirical values can be determined by making use of the low- and high-pressure limiting forms of eq 12.

If dissociation to new products (channel 10c) can be neglected, at low pressure ($k_E \gg \omega$) k_{loss} reduces to the third-order rate constant

$$k_0 = \frac{l_a}{l_b} \frac{q_{tr}^*}{q_A q_B} e^{-E_a/RT} Z_{LJ} \beta_c \int_0^\infty N(E) e^{-E/RT} dE \quad (15)$$

eliminating any dependence on the molecular properties of the transition state. An empirical value for E_0 can thus be obtained by calculating k_0 for chosen values of β_c and the collision cross section, σ_{LJ} , as a function of E_0 until agreement with the observed k_0 is obtained.

At high pressure ($\omega \gg k_E, k_E'$), k_{loss} is sensitive to the moments of inertia and vibrational frequencies of the transition state as

$$k_\infty = \frac{\alpha \kappa_b}{h} \frac{q_{tr}^\dagger}{q_A q_B} e^{-E_a/RT} \int_0^\infty \sum P(E^+) e^{-E^+/RT} dE^+ \quad (16)$$

Adjusting the vibrational frequencies of the transition state for a given set of moments of inertia to fit the high-pressure limit of k_{loss} provides an empirical, self-consistent set of parameters which can be used to calculate k_{loss} as a function of temperature. Since the high-pressure limit is often experimentally unattainable, fitting k_{loss} over a broad enough pressure range can often sufficiently define a valid set of parameters.

Calculation of Rate Constants. The monotonic decrease of the rate constant for the reaction of CH + N₂ with temperature between 297 and 675 K indicates that the addition reaction proceeds with either a very small or no activation energy. The endoergic abstraction reaction ($\Delta H = 3.7$ kcal/mol)¹⁸ which should have an added barrier, E_a' , as a result of the curve crossing necessitated by the spin change involved, will be competitive with addition only at higher temperatures. The data between 297 and 675 K were fitted first treating only the addition reaction. An estimate of E_a' was obtained by extending the calculations to higher temperatures using the results of Blauwens et al.³

Determination of E_0 . As seen previously (section IV) the collision efficiencies of Ar and N₂ were found to be equal; thus, a single value of β_c is used and $[M] = [Ar] + [N_2]$. $\langle \Delta E \rangle$ for this reaction was estimated from $\langle \Delta E \rangle$ values for other reaction systems¹⁹ involving a small number (four to eight) of atoms: $I + NO_2 \rightarrow INO_2$, $CH_3NC \rightarrow CH_3CN$, $CH_3 + CF_3 \rightarrow C_2F_3H_3$. These reactions have values of $-\langle \Delta E \rangle$ averaged for Ar and N₂ bath gases of 0.9, 0.8, and 0.9 kcal/mol at 300, 554, and 300 K, respectively. A value of $-\langle \Delta E \rangle$ of 1 kcal/mol ($\beta_c = 0.49$ at 297 K) was therefore used for most calculations along with a collision cross section of 4.0 Å. The effect of $\langle \Delta E \rangle$ on the calculations will be discussed later.

The molecular properties of the adduct used in the calculations were based on structures corresponding to diazomethane with one H atom removed. Calculations were performed for a linear CNN chain with the H atom either linear with the chain or bent with an HCN angle of 120°. Bond lengths, taken to be the same as in diazomethane,²⁰ and moments of inertia for these geometries are listed in Table III along with these parameters for the reactants. Vibrational frequencies for the adduct were

(18) D. R. Stull and H. Prophet et al., "JANAF Thermochemical Tables", 2nd ed., National Bureau of Standards, U.S. Government Printing Office, Washington, DC, 1971.

(19) J. Troe, *J. Phys. Chem.*, **83**, 114 (1979).

(20) G. Herzberg, "Molecular Spectra and Molecular Structure, III. Electronic Spectra of Polyatomic Molecules", Van Nostrand-Reinhold, New York, 1966.

(16) D. M. Bishop and K. J. Laidler, *J. Chem. Phys.*, **42**, 1688 (1965).

(17) J. Troe, *J. Chem. Phys.*, **66**, 4745 (1977).

TABLE III: Molecular Parameters for the Adduct and Reactants Used in Calculations

	CH	N ₂	HCN ₂
vibrational frequencies, cm ⁻¹	2733	2330	3130, ^a 2102, 1252, ^b 1170, 564, 421, 406 ^c
bond lengths, Å			
r _{CH}	1.1199		1.08
r _{NN}		1.0977	1.12
r _{CN}			1.32
moments of inertia, 10 ⁻⁴⁰ g cm ²	1.935	13.998	73.2 ^d 1.32, ^e 69.3, ^e 70.6 ^e

^a Geometric mean of CH stretch frequencies in diazomethane. ^b Geometric mean of CH₂ deformation and rock modes in diazomethane. ^c This mode (CH₂ wag in diazomethane) was removed for the nonlinear adduct. ^d For the linear adduct. ^e For the nonlinear adduct, HCN angle = 120°.

taken as geometric means of the corresponding frequencies^{20,21} in diazomethane with appropriate degeneracies and are also listed in Table III.

In calculations of k_0 , the density of states of the adduct was evaluated as $N(E) = N^{\text{WR}}(E)F_{\text{anh}}$ where $N^{\text{WR}}(E)$ is the harmonic density of states evaluated by the Whitten-Rabinovitch approximation¹⁵ and $F_{\text{anh}} = [(s-1)/(s-3/2)]^m$ is an anharmonicity correction factor²² for a molecule of s Morse oscillators of which $s-m$ remain in the products. $F_{\text{anh}} = 1.545$ and 1.524 , respectively, for decomposition of the linear and nonlinear adducts to CH and N₂. The anharmonicity correction was not included in calculations of k_{loss} since in those calculations transition-state properties must be considered and the anharmonicity of the transition-state vibrational frequencies, which would tend to cancel the effect of the anharmonicity of the adduct on k_{loss} , could not be easily incorporated.

Rate constants were calculated for the appropriate temperature and pressure by integration of eq 12 from $E^+ = 0$ to 99 kcal/mol in 0.1 kcal/mol intervals. A plot of the calculated k_0 as a function of E_0 is shown in Figure 8. The average of k_0 determined here (Figure 5) and that of Wagal et al.¹³ gave $k_0 = 2.7 \times 10^{-31}$ cm⁶ molecule⁻² s⁻¹, which was fitted well by $E_0 = 53$ kcal/mol for the linear adduct with $-\langle\Delta E\rangle = 1.0$ kcal/mol. $E_0 = 57$ and 61 kcal/mol were found for the linear adduct with $-\langle\Delta E\rangle = 0.5$ kcal/mol and the nonlinear adduct with $-\langle\Delta E\rangle = 1.0$ kcal/mol, respectively. The effect of $\langle\Delta E\rangle$ and geometry on E_0 will be discussed later. If an activation energy of $E_a = 1$ kcal/mol was assumed for the addition reaction, $E_0 = 72$ kcal/mol was required to fit k_0 .

Pressure and Temperature Dependence. Equation 12 was used to calculate k_{loss} as a function of total pressure. For the association reaction and its reverse, the transition-state geometry was chosen as that of the adduct with a lengthened C-N bond. The sum of vibrational states of the transition state, $\sum P(E^+)$, was calculated by direct count up to $E^+ = 15$ kcal/mol above which the Whitten-Rabinovitch approximation¹⁵ was used. A loose transition state, i.e., one with several very low frequency vibrational modes, was required for the calculated k_{loss} to match the curvature of the pressure-dependence plot (Figure 3). The C-H and N-H stretching frequencies were taken from the vibrational frequencies of the isolated diatomic species²³ while the remaining low-frequency modes were adjusted

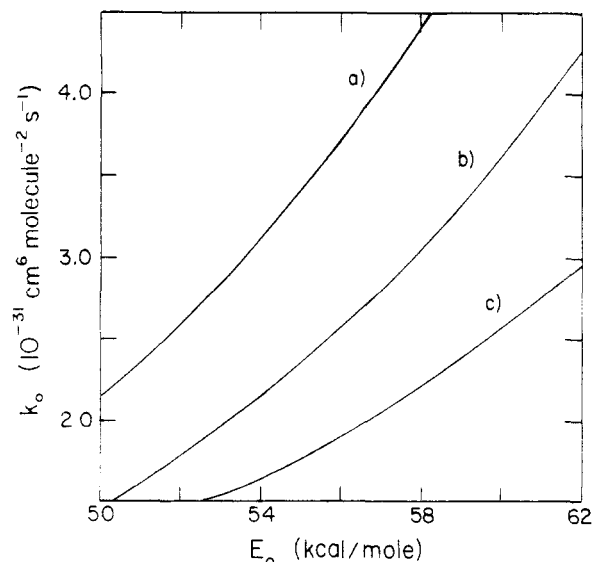


Figure 8. Plot of the calculated k_0 vs. E_0 for (a) parameter set I, (b) parameter set II, and (c) parameter set V.

for a particular transition-state geometry until a satisfactory fit was obtained. The frequencies used for several different transition-state geometries and deactivation efficiencies are listed in Table IV. Figure 3 shows the fits obtained for linear transition states with C-N bond lengths of $r_{\text{CN}} = 1.8$ Å corresponding to a Pauling bond order²⁴ of 0.16 and $r_{\text{CN}} = 4.0$ Å (parameters set III), the maximum of the centrifugal potential calculated as described by Tschuikow-Roux.²⁵ Both curves fit the data well except below 50 torr, where they underestimate the observed rate constant. The curves, however, are in the range defined by the data of Wagal et al.¹³ in this pressure range.

It is clear from Figure 3 that the highest experimental pressure, 787 torr, is far from the high-pressure limit for this reaction. Calculations predict a half-pressure (where $k = 1/2 k_{\infty}$) of $P_{1/2} = 3 \times 10^4$ torr. Although a more reliable set of transition-state frequencies would be obtained by fitting to k_{∞} , constraining the calculated pressure-dependence curve to pass through the error bars of the data above 50 torr limited the calculated k_{∞} to the range $k_{\infty} = (2 \pm 1) \times 10^{-11}$ cm³ molecule⁻¹ s⁻¹. This small range of k_{∞} indicates that the observed data restrict the set of transition-state vibrational frequencies sufficiently such that a precise value of k_{∞} , unless substantially outside the above range, should have little significant effect on the set of vibrational frequencies determined.

Using the parameters listed in Table IV, we calculated k_{loss} as a function of temperature in the range 297–1000 K for a total pressure of 100 torr and the results are shown in Figure 6. Curve a was calculated for a temperature-dependent β_c as defined in eq 14 with $-\langle\Delta E\rangle = 0.5$ kcal/mol (parameter set II). Calculations using $-\langle\Delta E\rangle = 1.0$ kcal/mol with $r_{\text{CN}} = 1.8$ and 4.0 Å, respectively (parameter sets I and III), produced very similar curves with k_{loss} becoming slightly larger than curve a at higher temperatures: 0.7% larger at 297 K and 11.2% larger at 675 K for parameter set I while parameter set III ranged from 13.2% to 16.4% larger than curve a at 297 and 675 K.

Curve b was obtained for the nonlinear adduct and transition state (parameter set V). The curve produced by using parameter set I with a temperature-independent $\beta_c = 0.49$, determined for $-\langle\Delta E\rangle = 1.0$ kcal/mol at 297 K,

(21) C. B. Moore and G. C. Pimentel, *J. Chem. Phys.*, **40**, 342 (1964).

(22) J. Troe, *J. Chem. Phys.*, **66**, 4758 (1977).

(23) K. P. Huber and G. Herzberg, "Molecular Spectra and Molecular Structure, IV. Constants of Diatomic Molecules", Van Nostrand-Reinhold, New York, 1979.

(24) H. S. Johnston, "Gas Phase Reaction Rate Theory", Ronald Press, New York, 1966.

(25) E. Tschuikow-Roux, *J. Phys. Chem.*, **72**, 1009 (1968).

TABLE IV: Parameters Used in Calculations of k_{loss}^a

parameter set	$-\langle\Delta E\rangle$, kcal/mol	E_a , kcal/mol	E_o , kcal/mol	I_{adduct} , g cm ²	I_{TS} , g cm ²	ν_{TS} , ^b cm ⁻¹
I	1.0	0.0	53	73.2	104.3	100 (1), 75 (3)
II	0.5	0.0	57	73.2	104.3	100 (1), 75 (3)
III	1.0	0.0	53	73.2	334.1	200 (2), 125 (2)
IV	1.0	1.0	72	73.2	104.3	40 (4)
V	1.0	0.0	61	1.32	1.32	300 (1), 200 (2)
				69.3	108.6	
				70.6	109.9	

^a Calculations use $l_a = 2$, $l_b = 1$, $l_c = 1$, $g_{\text{CH}} = 2$, $g_{\text{N}_2} = 1$, $g_{\text{HCN}_2} = 2$. I_{adduct} and I_{TS} are the moments of inertia of the adduct and transition state b, respectively. ^b The ν_{TS} are the vibrational frequencies of transition state b. All parameter sets also have transition-state vibrational frequencies = 2733 and 2330 cm⁻¹. Degeneracies are in parentheses.

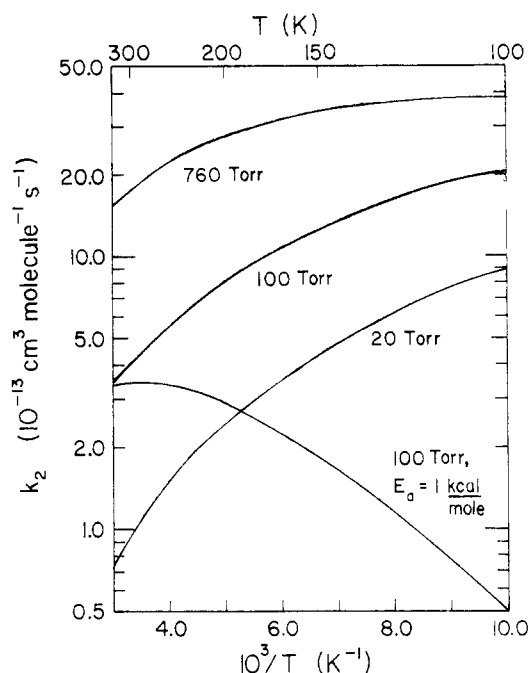


Figure 9. Arrhenius plot of the calculated second-order rate constant for the CH + N₂ reaction at several total pressures. Parameter set I is used except where noted.

is similar to curve b, ranging from 12% lower at 297 K to 3.9% larger at 675 K. A similar curve is obtained with parameter set II with a constant $\beta_c = 0.34$.

There is qualitative agreement between the calculations and the experimental data, all displaying a concave downward curvature in the negative temperature dependence of the Arrhenius plot. Agreement at the low-temperature end is constrained as the transition-state parameters were adjusted to reproduce the data at 297 K. At higher temperatures the data are fitted somewhat better for the smaller value of $|\langle\Delta E\rangle|$. For the same parameter set, the curve employing a temperature-dependent β_c gave much better quantitative agreement than that for a constant β_c or for the linear least-squares fit. The disparity between curve b and the data, however, may be due in part to the choice of the correct functional form^{17,19} of the temperature dependence of β_c or the magnitude of $\langle\Delta E\rangle$. Inclusion of a 1 kcal/mol activation energy for the addition reaction (curve c) counteracts the negative temperature dependence arising from the loss of translational and rotational degrees of freedom upon formation of the adduct leading to poor quantitative agreement with the data.

The extension of these calculations to lower temperatures relies on the magnitude of E_a . Figure 9 shows the Arrhenius plot for the CH + N₂ reaction in the 100–300 K region for $E_a = 0$ and 1.0 kcal/mol. The former predicts a continuous negative temperature dependence to at least

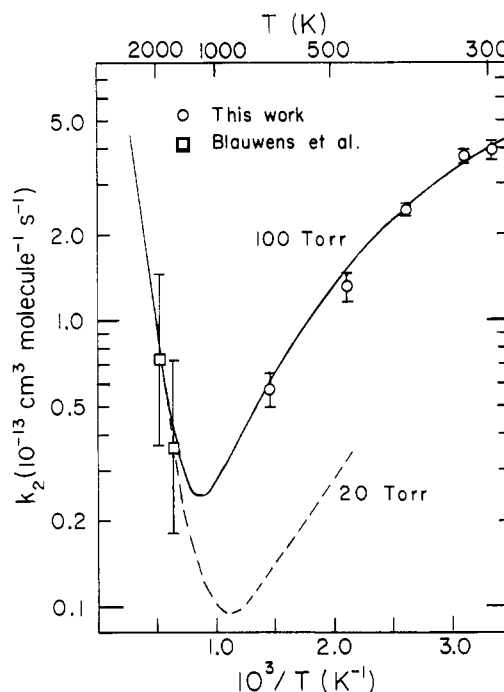


Figure 10. Arrhenius plot of data from this work (O) at 100 torr and that of Blauwens et al.³ (□) at 18–40-torr total pressure for the CH + N₂ reaction. Only rate constants evaluated at the limiting flame front temperatures in their work are shown. The solid curve is the result of transition-state-theory calculations for 100-torr total pressure, the dashed curve for 20-torr total pressure, both curves using parameter set II.

100 K while the latter shows an inflection at about 270 K. The parameters for the latter, however, did not accurately represent the temperature dependence at higher temperatures and should set a lower limit to the rate constant in the lower temperature range. Centrifugal effects dependent on rotational quantum numbers were not included in the calculations.

At higher temperatures, the abstraction pathway, channel 10c, must be considered. Blauwens et al.³ proposed that the appearance of prompt NO in hydrocarbon/air flame fronts could be attributed to either reaction 1 with $k = (1.3 \times 10^{-12}) \exp(-11000/RT)$ cm³ molecule⁻¹ s⁻¹ or reaction 3 with $k = (4.7 \times 10^{-12}) \exp(-22500/RT)$ cm³ molecule⁻¹ s⁻¹. The values of the rate constant for reaction 1 at the limiting flame front temperatures used in that study are shown in Figure 10 with the quoted factor of 2 error ($2k > k > 0.5k$).

In order to test the compatibility of this previous determination of the rate constant for the CH + N₂ reaction with our lower temperature observations we have performed calculations which included the abstraction channel up to 3333 K. For simplicity, the transition state for abstraction was taken as a linear²⁶ HCN with an extended

N–N bond length of $r_{\text{NN}} = 1.3 \text{ \AA}$. Vibrational frequencies were taken as geometric averages of diazomethane frequencies with the N–N stretching mode removed as the reaction coordinate. The energy barrier for this reaction relative to reactants, $\Delta E_0 + E_a'$, and κ_c were varied so the calculated k_{loss} would fit the rate constants of Blauwens et al.³ Figure 10 shows the curve obtained for $\Delta E_0 = 3.7 \text{ kcal/mol}$, $E_a' = 3.3 \text{ kcal/mol}$, $\kappa_c = 0.5$, and parameter set II from Table IV at two total pressures. The calculated Arrhenius plot shows a pressure-dependent inflection point due to the competition between abstraction and collisional stabilization of the adduct. At temperatures above 1500 K with pressures below 760 torr the abstraction reaction is dominant and k_{loss} is pressure independent. The resulting slope of the Arrhenius plot corresponds to experimental activation energies of $-R[d \ln k/d(1/T)] = 12 \text{ kcal/mol}$ between 1500 and 2500 K and 18 kcal/mol between 2500 and 3333 K. These calculations can thus provide good agreement with both our data and those from flames interpreted with reaction 1 as the main route for production of prompt NO.

VI. Discussion

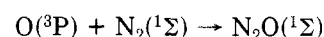
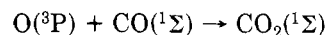
Comparison with Previous Work. The room-temperature rate constants observed here at 25 and 50 torr are in agreement with the recent results of Wagal et al.,¹³ who worked at total pressures between 2 and 75 torr. Their rate constant for a total pressure of 100 torr, $k_{100} = (3.66 \pm 0.27) \times 10^{-13} \text{ cm}^3 \text{ molecule}^{-1} \text{ s}^{-1}$, is in good agreement with our measured value of $k_{100} = (3.9 \pm 0.3) \times 10^{-13} \text{ cm}^3 \text{ molecule}^{-1} \text{ s}^{-1}$. Our extrapolated value of $k_0 = (2.8 \pm 0.5) \times 10^{-31} \text{ cm}^6 \text{ molecule}^{-2} \text{ s}^{-1}$ is also in good agreement with their value of $2.6 \times 10^{-31} \text{ cm}^6 \text{ molecule}^{-2} \text{ s}^{-1}$. Their extrapolation to $k_\infty = (6.3 \pm 1.3) \times 10^{-13} \text{ cm}^3 \text{ molecule}^{-1} \text{ s}^{-1}$, however, is a factor of 30 lower than that determined here. Rate constants measured here at 200-torr total pressure already exceed their value of k_∞ . It is clear that higher pressure data are required to see sufficient curvature in the falloff plot for satisfactory extrapolation. Our RRKM calculations indicate that the high-pressure limit will be reached at pressures in the range of 10^4 atm . Our calculated value of $k_\infty = (2 \pm 1) \times 10^{-11} \text{ cm}^3 \text{ molecule}^{-1} \text{ s}^{-1}$ is in the range of the limiting high-pressure rate constants observed for other molecular recombination reactions.²⁷

The rate constants observed by Butler et al.⁸ display a pressure dependence similar to those observed here; however, their absolute rate constants are 2.2–2.5 times slower at each pressure. A similar systematic discrepancy was observed for other pressure-dependent rate constants for CH radical reactions.¹⁴

Braun et al.¹¹ reported a second-order rate constant of $k = 7.1 \times 10^{-14} \text{ cm}^3 \text{ molecule}^{-1} \text{ s}^{-1}$ at 298 K for measurements in which the total pressure ranged between 1 and 40 torr of mostly N_2 ; however, only one measurement was at a pressure greater than 20 torr. This rate constant is consistent with both our results and the work of Wagal et al.¹³ at pressures between 10 and 20 torr. Bosnali and Perner,¹² using 15 torr of methane as a CH precursor, gave a second-order rate constant of $k = (1.0_{-0.5}^{+0.2}) \times 10^{-12} \text{ cm}^3 \text{ molecule}^{-1} \text{ s}^{-1}$; however, they did not report the total pressure range. Our results show that an average total pressure of about 300 torr would produce a rate constant of $k = 1 \times 10^{-12} \text{ cm}^3 \text{ molecule}^{-1} \text{ s}^{-1}$.

The temperature dependence of the CH + N_2 reaction between 297 and 675 K is very similar to that observed¹⁴

for the reaction of CH + CO, having Arrhenius activation energies of -1.97 ± 0.13 and $-1.72 \pm 0.20 \text{ kcal/mol}$, respectively. Both reactions appear to proceed via addition mechanisms in this temperature range above pressures of 25 torr. The barriers to the abstraction reactions in these cases are determined by the reaction endoergicities and additional barriers such as that due to the curve crossing in reaction 1 necessitated by the spin change involved. The probability for such a crossing is expected to be large as formation of a long-lived complex provides the opportunity for multiple curve crossings^{28,29} between doublet and quartet potential surfaces of the HCN_2 adduct. In CH, the $^4\Sigma$ state lies 17 kcal/mol above the ground-state doublet.³⁰ Other reactions involving a spin change such as



have activation energies of about 5³¹ and 20–23^{32,33} kcal/mol, respectively, arising from curve crossings.

On the basis of our data and the results of Blauwens et al.³ we calculated, for a 3.7 kcal/mol endoergicity, a crossing barrier of 3.3 kcal/mol. The competition between abstraction and adduct stabilization gives rise to a pressure-dependent inflection point in the Arrhenius plot occurring at $\sim 1000 \text{ K}$ for CH + N_2 at a total pressure of 100 torr. The CH + CO \rightarrow C₂O + H reaction is endoergic by from 5 ± 15 ¹⁸ to 30 ± 5 ³⁴ kcal/mol and calculations similar to those described for CH + N_2 using the latter endoergicity indicate an inflection point in the range of 2000–3000 K at 100 torr. In contrast, the CH + $\text{H}_2 \rightarrow$ CH₂ + H reaction is endoergic by only 2.7 kcal/mol and an inflection point has been experimentally observed³⁵ at $\sim 450 \text{ K}$ for a total pressure of 100 torr.

Other systems that show similar temperature dependences are the reactions of OH + benzene and related aromatic compounds.^{36,37} As in the CH + N_2 system, abstraction and adduct stabilization compete, producing inflected Arrhenius plots. In the OH systems, decomposition of the thermalized adduct has been proposed to explain nonexponential behavior observed in the decay of the OH concentration in the 325–380 K temperature range. Activation energies of 18–19 kcal/mol for these processes were determined.³⁶ Our calculations of E_0 show the HCN_2 adduct to be thermodynamically stable to dissociation by about 50–60 kcal/mol. Decomposition of the thermalized adduct, therefore, is prevented at these temperatures and

(28) J. C. Tully, *J. Chem. Phys.*, **61**, 61 (1974).

(29) G. E. Zahr, R. K. Preston, and W. H. Miller, *J. Chem. Phys.*, **62**, 1127 (1975).

(30) A. Kasdan, E. Herbst, and W. C. Lineberger, *Chem. Phys. Lett.*, **31**, 78 (1975); P. F. Zittel and W. C. Lineberger, *J. Chem. Phys.*, **65**, 1932 (1976).

(31) T. G. Slanger, B. J. Wood, and G. Black, *J. Chem. Phys.*, **57**, 233 (1972); H. Gg. Wagner and F. Zabel, *Ber. Bunsenges. Phys. Chem.*, **78**, 705 (1974).

(32) H. A. Olschewski, J. Troe, and H. Gg. Wagner, *Ber. Bunsenges. Phys. Chem.*, **70**, 450 (1966).

(33) S. W. Benson and H. E. O'Neal, "Kinetic Data on Gas Phase Unimolecular Reactions", National Bureau of Standards, U.S. Government Printing Office, Washington, DC, 1970.

(34) Using $\Delta H_f(0 \text{ K}, \text{C}_2\text{O}) = 93 \pm 5$ from C. Willis and K. D. Bayes, *J. Phys. Chem.*, **71**, 3367 (1967).

(35) M. R. Berman, J. W. Fleming, and M. C. Lin in "Lasers as Reactants and Probes in Chemistry", W. M. Jackson and A. B. Harvey, Eds., Howard University Press, Washington, DC, in press; M. R. Berman and M. C. Lin, to be submitted for publication.

(36) R. A. Perry, R. Atkinson, and J. N. Pitts, *J. Phys. Chem.*, **81**, 296, 1607 (1977).

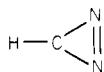
(37) F. P. Tully, A. R. Ravishankara, R. L. Thompson, J. M. Nicovich, R. C. Shah, N. M. Kreutter, and P. H. Wine, *J. Phys. Chem.*, **85**, 2262 (1981); J. M. Nicovich, R. L. Thompson, and A. R. Ravishankara, *ibid.*, **85**, 2913 (1981).

(26) B. R. Brooks and H. F. Schaefer, *J. Chem. Phys.*, **67**, 5146 (1977).

(27) J. Troe, "15th Symposium (International) on Combustion", The Combustion Institute, Pittsburgh, PA, 1975, p 667.

exponential decay of the CH concentration was observed throughout the temperature range studied.

Transition-State-Theory Calculations. While clearly it is quite difficult to calculate absolute rate constants from transition-state theory, calculations of k_0 should be fairly reliable since it is independent of transition-state parameters. Determination of E_0 is dependent on the collisional deactivation rate and the molecular properties of the adduct. Several geometries for the adduct can be proposed. The HCNN³⁸ and HNCN³⁹ radicals have both been observed spectroscopically. For the latter, the NCN chain was found to be linear with its length within 0.01 Å of the CNN distance in diazomethane. The HNC bond angle was 116°. No vibrational frequencies were determined. Some unassigned vibrational absorption lines have been observed for HCNN.³⁸ A small deviation of the CNN bond angle from 180° has been suggested.⁴⁰ Triangular



is also a plausible structure for the adduct; however, a large barrier is expected for the least-motion pathway of CH approaching perpendicular to the bisector of the internuclear axis of N₂ similar to the 75 kcal/mol barrier calculated²⁶ for this approach for CH + H₂. The HCNN configuration was chosen due to the availability of assigned vibrational frequencies and moments of inertia for diazomethane. The choice of particular configuration should not have a significant effect on the calculated temperature dependence.

An empirical determination of E_0 is required since the heat of formation and the C-H bond energy for diazomethane are not well-known. Laufer and Okabe⁴¹ found $\Delta H_f^\circ(\text{CH}_2\text{N}_2) \geq 51.3$ kcal/mol while Benson⁴² lists $\Delta H_f^\circ_{300} = 71$ kcal/mol. A value of $E_0 = 53$ kcal/mol for HCN₂ with Laufer and Okabe's lower limit corresponds to a C-H bond energy in diazomethane of 90 kcal/mol, which is not an unreasonable value. A C-H bond energy of 93 ± 2.5 kcal/mol was reported for H₃C-CN.⁴³ Comparison with radicals containing an α -cyano group indicates that resonance stabilization of the radical should be <5 kcal/mol.⁴³ Values of $E_0 > 65$ kcal/mol or $\Delta H_f^\circ(\text{CH}_2\text{N}_2) = 71$ kcal/mol require unreasonably small values for the C-H bond energy in diazomethane. Calculations using $E_a = 1$ kcal/mol lead to a value of $E_0 = 71$ kcal/mol. A smaller activation energy for the association reaction is required to produce a value of E_0 consistent with a reasonable CH bond strength in diazomethane. The poor agreement with the temperature-dependence data for calculations using $E_a = 1$ kcal/mol supports this conclusion that $E_a < 1$ kcal/mol.

Calculated fits to the observed pressure dependence required the use of several very low frequency vibrational modes for the transition state (see Table IV). Prediction of a loose transition state implies that alternate transition-state models incorporating free rotation may be applicable. The model employed here simply demonstrates that a satisfactory description of the observed data at both low and high temperatures can be obtained with the mechanism of eq 10. The calculations performed in section V by no means confirm or preclude a particular set of

parameters, i.e., collision efficiency, geometry, or sets of vibrational frequencies for the adduct or transition states. They do, however, provide a useful, self-consistent means for describing the data and judging the compatibility of the results of this work with others as well as providing a basis for cautious extrapolation of the results to different temperature ranges.

The empirical fit of the transition-state vibrational frequencies to the pressure dependence at room temperature constrains the temperature fits near 300 K. Agreement at other temperatures relies on the temperature dependence of the collision efficiency, β_c . Figure 6 demonstrates the substantially improved fit obtained by using a temperature-dependent β_c as defined in eq 14 as opposed to using a constant β_c . Since eq 14 was derived for a thermally activated system, the narrow distribution characteristic of chemical activation may lead to a larger β_c than calculated by eq 14. The predicted temperature dependence of β_c is nonetheless useful in fitting the data. The temperature- and pressure-dependence calculations of k_{loss} were relatively insensitive to the magnitude of $\langle \Delta E \rangle$ and, hence, β_c . Only a 12% difference in k_{loss} was calculated between $-\langle \Delta E \rangle = 0.5$ and 1.0 kcal/mol at 675 K ($\beta_c = 0.19$ and 0.30, respectively). A slightly larger negative slope in the Arrhenius plot and improved agreement with the data were obtained by using $-\langle \Delta E \rangle = 0.5$ kcal/mol. The magnitude of the calculated E_0 is also dependent on $\langle \Delta E \rangle$ and β_c . Increasing E_0 and, hence, the density of states compensates for a smaller β_c in calculating k_0 . A considerably smaller value for β_c such as $\beta_c = 0.04$ reported²² for O₃ decomposition at 300 K would require an unreasonably large value of E_0 (>70 kcal/mol) to fit the data.

Application to Combustion and Planetary Atmosphere Systems. Reaction 10 provides a unified mechanism that successfully describes the CH + N₂ reaction over a broad temperature range. It is favored over reaction 3 as the source of NO in hydrocarbon/air flame fronts for several reasons. The 7 kcal/mol barrier (above CH + N₂) to abstraction required in our calculations to fit the data of Blauwens et al., as shown earlier, is reasonable for this reaction despite the spin change involved since the reaction proceeds through a long-lived complex. Calculations similar to those described in section V were performed for reaction 3 proceeding through an excited diazomethane intermediate, employing $\Delta E_0 = 24$ kcal/mol between reactants, CH₂(X³B₁) and N₂, and products, HCN and NH(X³Σ⁻), with no additional energy barrier. An Arrhenius activation energy of ~ 30 kcal/mol was found. Formation of these products, however, from an H₂CNN complex requires a highly strained geometry which would create an even larger energy barrier. On structural and energetic grounds, Benson⁹ suggested that the reaction of CH₂ + N₂ in flames would result in formation and redissociation of the H₂CNN adduct. The endoergicity of the next higher energy channel open to the adduct, production of H₂CN + N, is prohibitively large (≥ 80 kcal/mol). A significantly smaller activation energy of only 22.5 kcal/mol for reaction 3 was required by Blauwens et al. to fit their data with this reaction. The low A factor and high activation energy for the direct four-center mechanism⁹ similarly make this reaction appear less probable than reaction 1 for describing NO production in these flame fronts.

The CH + N₂ reaction clearly proceeds by the addition mechanism at lower temperatures. The rate constant for the metathesis at 300 K is $k = 10^{-20}$ cm³ molecule⁻¹ s⁻¹ based on extrapolation of the results from the work in

(38) J. F. Ogilvie, *Can. J. Chem.*, **46**, 2472 (1968).

(39) G. Herzberg and P. A. Warsop, *Can. J. Phys.*, **41**, 286 (1963); N. Basco and K. K. Yee, *Chem. Commun.*, 150 (1968).

(40) T. Fueno, private communication.

(41) A. H. Laufer and H. Okabe, *J. Am. Chem. Soc.*, **93**, 4137 (1971).

(42) S. W. Benson, "Thermochemical Kinetics", Wiley, New York, 1976.

(43) D. F. McMillen and D. M. Golden, *Annu. Rev. Phys. Chem.*, **33**, 493 (1982).

flames. Calculations of the rate constant at the low temperatures of interest to certain planetary atmospheres are sensitive to small activation energies for the association reaction, due perhaps to centrifugal effects. A small E_a would reduce and, at low enough temperatures, eventually invert the negative temperature dependence. A 1 kcal/mol barrier, however, appears to be too large. The rate constants calculated for zero activation energy provide an upper limit to the true rate constant at a particular total pressure. The rate of increase of this limiting rate constant decreases with increasing pressure so that, at 760 torr, the rate constant increases by only a factor of 2 between 300 and 100 K. On the basis of its similarity to diazomethane, the fate of the stabilized HCN_2 adduct in planetary atmospheres is most likely photodissociation back to CH and N_2 .

VII. Conclusion

The reaction of $\text{CH} + \text{N}_2$ is dominated by two different reaction channels in different temperature ranges. At low temperatures, the reaction is dominated by the addition mechanism. This results in a pressure-dependent, second-order rate constant with a negative temperature dependence. Disparity between previous measurements may well be due to the effect of pressure on the rate constant. At high temperatures, the endoergic abstraction channel or metathesis becomes the primary reaction pathway.

A unified mechanism involving formation of an excited HCN_2 intermediate followed by competition between collisional stabilization of the adduct and decomposition to either $\text{HCN} + \text{N}$ products or $\text{CH} + \text{N}_2$ reactants successfully describes experimental observations. The competition between reaction channels results in an Arrhenius plot containing regions of positive and negative slope separated by a pressure-dependent inflection point. Arrhenius parameters from a linear least-squares fit listed for the addition reaction rate constant are valid as an approximation to the temperature dependence only over a limited temperature range and only for a total pressure of 100 torr.

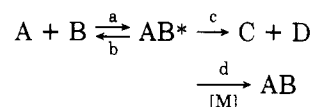
Calculations of the reaction rate constant using a transition-state-theory model with the RRKM theory applied to the unimolecular dissociation of the chemically activated adduct have provided a self-consistent description of the pressure and temperature dependences of this reaction. Use of a weak-collision approximation in the form of a temperature-dependent collision efficiency factor, β_c , produced good agreement between the temperature dependences of the rate constant calculated and observed experimentally. Calculations based on our data and the work of Blauwens et al. are consistent with reaction 10 being the source of the NO produced in the reaction zones of hydrocarbon/air flames.

Acknowledgment. We thank T. Carrington, S. V. Filseth, and co-workers for providing us their results prior

to publication. Partial support for this work from the NASA Planetary Atmospheres Program Office is gratefully acknowledged.

Appendix

For a bimolecular reaction occurring via a stable intermediate



the rate constant for the loss of reactant A in the steady-state approximation for AB^* is given by

$$k_{\text{loss}} = \frac{-d[\text{A}]/dt}{[\text{A}][\text{B}]} = \frac{k_b K_{\text{ab}}(k_c + k_d[\text{M}])}{k_b + k_c + k_d[\text{M}]} \quad (\text{A1})$$

Since the freshly formed intermediate AB^* contains energy $E = E_0 + E_a$, the rate constants k_a , k_b , and k_c , and therefore K_{ab} , are all functions of internal energy. Hence, we write $k_E = k_b$, $k_E' = k_c$, and $K_E = K_{\text{ab}}$. Employing the weak-collision approximation, the effective collisional deactivation rate constant is $\omega = \beta_c Z_{\text{LJ}}[\text{M}] = k_d[\text{M}]$.

The equilibrium constant K_E can be evaluated at reaction temperature T by assuming that the overall rotational and translational degrees of freedom are "inactive" and separable from the vibrational modes. Thus, one has

$$K_E dE = \frac{Q_{\text{tr}}^* e^{-E_a/RT}}{Q_A Q_B} N(E) e^{-E^*/RT} dE^+ \quad (\text{A2})$$

where Q_A and Q_B are the total partition functions of reactants A and B, respectively, and Q_{tr}^* is the product of the translational and rotational partition functions of the intermediate AB. Electronic multiplicities are included in each partition function.

Inserting eq A2 and the rate constants given above into eq A1 followed by integration gives

$$k_{\text{loss}} = \frac{Q_{\text{tr}}^*}{Q_A Q_B} e^{-E_a/RT} \int_0^\infty \frac{(\omega + k_E') k_E}{k_E + k_E' + \omega} N(E) e^{-E^*/RT} dE^+ \quad (\text{A3})$$

The symmetry numbers, σ , from the partition functions can be extracted by employing the general relationship between them and the statistical factors¹⁶ for the reaction, $\sigma_A \sigma_B / \sigma_{\text{AB}^*} = I_a / I_b$. Inserting eq 13a, the RRKM rate constant expression¹⁵ for k_E , into the numerator of eq A3 and using $I_b = q_{\text{tr}}^\ddagger / q_{\text{tr}}^*$ and $\alpha = I_a g^\ddagger / g_{\text{AB}^*}$ gives

$$k_{\text{loss}} = \frac{\alpha k_b}{h} \frac{q_{\text{tr}}^\ddagger}{q_A q_B} e^{-E_a/RT} \int_0^\infty \frac{(\omega + k_E') \sum P(E^+)}{k_E + k_E' + \omega} e^{-E^*/RT} dE^+ \quad (\text{A4})$$

Registry No. CH, 3315-37-5; N_2 , 7727-37-9.